Three-dimensional inverse energy transfer induced by vortex reconnections

Andrew W. Baggaley,[1,*] Carlo F. Barenghi,[2,†] and Yuri A. Sergeev[3,‡]

[1]*School of Mathematics and Statistics, University of Glasgow, Glasgow, G12 8QW, United Kingdom*

[2]*Joint Quantum Centre Durham-Newcastle and School of Mathematics and Statistics, Newcastle University, Newcastle upon Tyne, NE1 7RU, United Kingdom*

[3]*Joint Quantum Centre Durham-Newcastle and School of Mechanical and Systems Engineering, Newcastle University, Newcastle upon Tyne, NE1 7RU, United Kingdom*

(Received 8 May 2013; revised manuscript received 23 October 2013; published 6 January 2014)

In low-temperature superfluid helium, viscosity is zero and vorticity takes the form of discrete vortex filaments of fixed circulation and atomic thickness. We present numerical evidence of three-dimensional inverse energy transfer from small length scales to large length scales in superfluid turbulence generated by a flow of vortex rings. We argue that the effect arises from the anisotropy of the flow, which favors vortex reconnections of vortex loops of the same polarity, and that it has been indirectly observed in the laboratory. The effect opens questions about analogies with related processes in ordinary turbulence.

DOI: 10.1103/PhysRevE.89.013002 PACS number(s): 67.25.dk, 47.27.Gs, 47.32.C−

The phenomenology of three-dimensional turbulence is based on Richardson's idea [1] of the (forward) turbulent cascade. Kinetic energy, injected externally at large length scales, feeds large unstable eddies, which interact, become stretched, and break up into smaller eddies. The process repeats until at sufficiently small length scales viscous forces dissipate energy into heat. A reversed flux of energy from the small scales to the large scales is observed in two-dimensional turbulence [2,3]. Such an inverse cascade is rare in three-dimensional turbulence, but can be observed in the presence of strong anisotropy [4–7] or when rotation [8–10] or stratification [11] makes the flow almost two dimensional. An example is Jupiter's Great Red Spot [12,13].

At temperatures below 1 K, thermal excitations can be neglected and liquid helium (^{4}He) is a pure superfluid. Unlike ordinary fluids (in which vorticity is a continuous field), the superfluid's rotational motion is constrained by quantum mechanics to discrete vortex lines of fixed circulation κ and atomic thickness (the radius of the vortex core is only $a_0 \approx 10^{-8}$ cm). Turbulence [14], easily excited by stirring the liquid helium, is a tangle of such vortex lines. An important property of vortex lines is that they reconnect when they come sufficiently close to each other, as predicted by theory [15–17] and observed in experiments [18]. Superfluid reconnections are similar to reconnections in ordinary fluids [19].

In this paper, we exploit the singular nature of superfluid vorticity to examine the three-dimensional inverse energy transfer. Using numerical simulations, first we demonstrate that an inverse energy transfer is possible in superfluid helium (and, we argue, it has already been observed in the laboratory, although indirectly). Second, we show that vortex reconnections play a key role in this process.

We numerically model vortex lines [20] as oriented space curves $\mathbf{s}(\xi,t)$ of infinitesimal thickness, where ξ is the arc length and t is time. This approach is justified by the large separation of scales between a_0 and the typical distance between vortices $\ell \approx L^{-1/2}$ (where $L = \Lambda/V$ is the vortex line density, Λ the vortex length, and V volume). Two physical ingredients determine the evolution of vortex lines. The first is Helmoltz's theorem: A vortex at location $\mathbf{s}$ is swept by velocity field $\mathbf{v}$ generated by the entire vortex configuration $\mathcal{L}$ at $\mathbf{s}$ via the Biot-Savart law [21]

$$\frac{d\mathbf{s}}{dt} = \mathbf{v}(\mathbf{s},t), \tag{1a}$$

$$\mathbf{v}(\mathbf{s},t) = -\frac{\kappa}{4\pi}\oint_{\mathcal{L}} \frac{(\mathbf{s}-\mathbf{r})}{|\mathbf{s}-\mathbf{r}|^3} \times \mathbf{dr}, \tag{1b}$$

where $\kappa = 9.97 \times 10^{-4}$ cm^2/s. The second ingredient, mentioned before, is vortex reconnections, instantaneous events that occur when vortex lines collide.

Our numerical simulations are performed in a periodic cube of size D. The techniques to discretize vortex lines into a variable number of points held at minimum separation $\delta/2$, time step Eq. (1a), desingularize the Biot-Savart integrals (1b), and evaluate them via a tree method [22] are described in the literature [23,24]. The reconnection algorithm is described in [25] and compared to other published algorithms.

In a pure superfluid, although viscosity is zero, the kinetic energy $K(t)$ is not conserved, but is turned into sound (phonons) by rapidly rotating Kelvin waves (helical perturbations of vortex lines) at length scales of the order of $10^2 a_0$ [26]. In our simulations it is impossible to discretize vortex lines down to almost the atomic scale. However, the finite numerical resolution qualitatively models phonon losses [27] because it damps out Kelvin waves at scales of the order of δ and slightly reduces the vortex length (again at scale δ) at each reconnection event. Kelvin waves are often studied in the context of the decay of superfluid turbulence at very low temperatures. Interacting Kelvin waves (see [28] and references therein) form a one-dimensional weakly nonlinear system in which a dual cascade in k space takes place: a direct cascade of energy to large k and an inverse cascade of wave action to small k [29]. Generation of long waves as well as short waves on individual vortices has been observed in numerical simulations [30], but this Kelvin cascade process

*andrew.baggaley@glasgow.ac.uk
†c.f.barenghi@ncl.ac.uk
‡yuri.sergeev@ncl.ac.uk

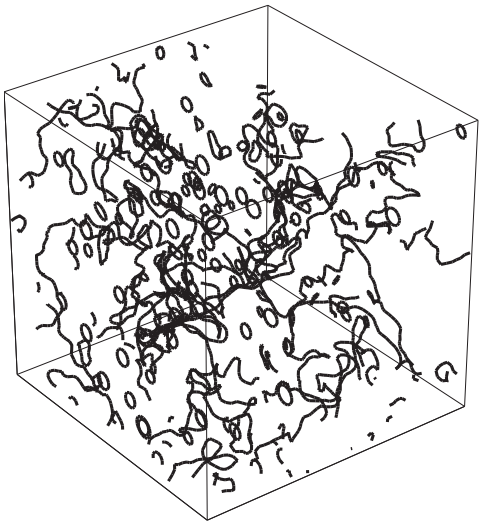

FIG. 1. First numerical simulation. Snapshots of the vortex tangle in the steady-state regime at $t = 4$ s ($L \approx 6000$ cm^{-2}).

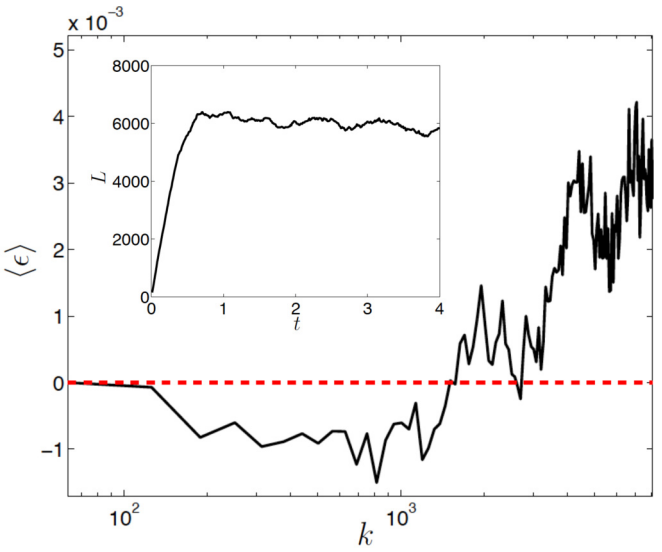

FIG. 2. (Color online) First numerical simulation. Energy flux $\langle\epsilon\rangle$ (averaged over the statistical steady regime $2 < t < 4$ s) vs wave number k (cm^{-1}). Notice that $\langle\epsilon\rangle < 0$ for $k < k_f$ (energy is transferred from small to large length scales) and $\langle\epsilon\rangle > 0$ for $k > k_f$ (energy is transferred from large to small scales), where $k_f \approx 1300$ cm^{-1} is the wave number corresponding to the average diameter of the injected rings. The inset shows the vortex line density L (cm^{-2}) vs time t (s).

is not directly relevant to the inverse energy transfer that we present here, which is three dimensional in nature.

Our first numerical simulation [31] models experiments [32]. We start with an empty computational box and inject vortex rings at frequency f drawing their radius from a normal distribution. The rings are in the yz plane and travel in the positive x direction; their evolution is computed using the full Biot-Savart law and the reconnection algorithm. After an initial transient, the vortex system settles to a statistical steady state. A snapshot of the vortex tangle is shown in Fig. 1. In this regime forcing is balanced by dissipation and the vortex line density fluctuates about a saturated value, as shown in the inset of Fig. 2.

To determine the distribution of the kinetic energy over the length scales, we Fourier transform [33] the velocity field $\mathbf{v}$ and define the energy spectrum $E(k)$ by

$$K(t) = \frac{1}{V}\int \frac{1}{2}\mathbf{v}^2 dV = \int_0^\infty E(k)dk, \qquad (2)$$

where $k = |\mathbf{k}|$ is the magnitude of the three-dimensional wave number and $V = D^3$ is the volume. Large (small) length scales correspond to small (large) wave numbers k, respectively. We find that, during the evolution, $E(k)$ progressively increases at small k. To quantify this energy transfer to large length scales, we compute the energy flux $\epsilon(k) = -\int_{k_D}^{k} dE(k')/dt\, dk'$ with $k_D = 2\pi/D$. Figure 2 shows that, in the statistically steady regime, the time-averaged energy flux $\langle\epsilon\rangle$ is negative for $k < k_f$ and positive for $k > k_f$, where $k_f = 2\pi/2\bar{R} \approx 1300$ cm^{-1} is the forcing wave number based on the injected rings' mean diameter $2\bar{R}$.

In other numerical simulations we examine the inverse energy transfer under different conditions. The second simulation [34] is inspired by numerical studies of homogeneous isotropic turbulence in which a forcing term is added to the governing Navier-Stokes equation to balance viscous dissipation and achieve a statistically steady state, independent of the initial condition. We add a random, incompressible, isotropic velocity field $\mathbf{v}_{\rm ext}$ to the right-hand side of Eq. (1a), consisting of 100 random Fourier modes, narrow banded ($\Delta k \approx 2$ cm^{-1}) around wave number $k_f \approx 70$ cm^{-1}, with $\langle \mathbf{v}_{\rm ext}^2 \rangle^{1/2} = 3.1$ cm/s. The seeding initial condition consists of a small number of randomly oriented vortex rings. During the evolution, energy is fed into the system by $\mathbf{v}_{\rm ext}$ and removed by the numerical dissipation. Figure 3 shows the growth of

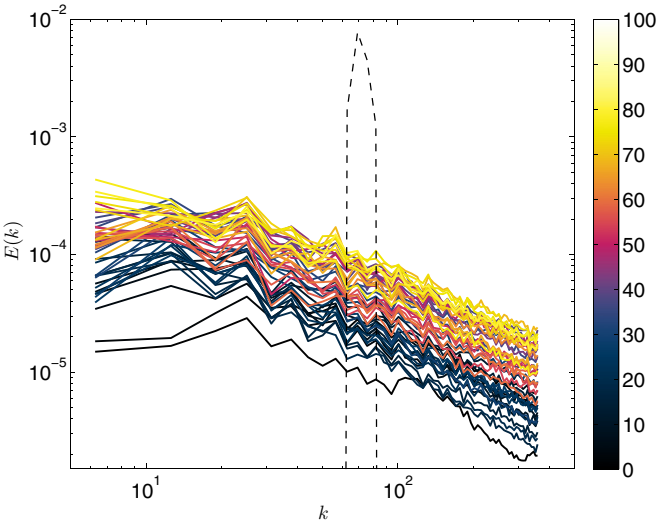

FIG. 3. (Color online) Second numerical simulation. Energy spectra $E(k)$ (arbitrary units) vs wave number k (cm^{-1}) shaded according to time t (s) as in the legend. The dashed line is the spectrum (arbitrary units, scaled for visibility) of the forcing term $\mathbf{v}_{\rm ext}$ with the maximum at $k = k_f$. Note the growth of the spectrum at all wave numbers, particularly for $k < k_f$.

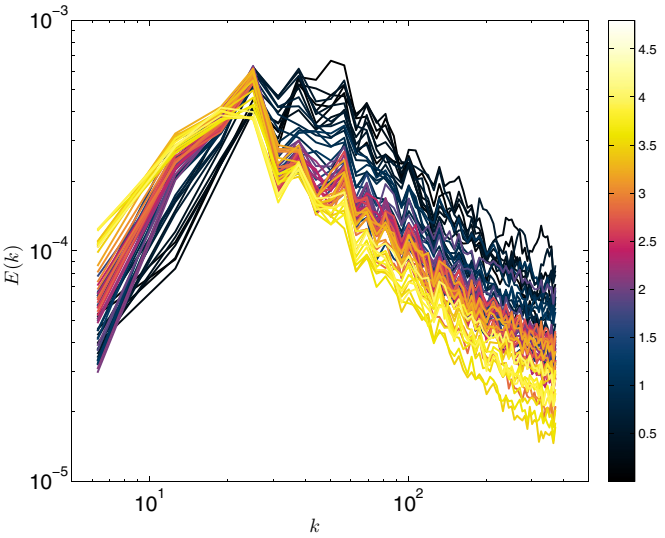

FIG. 4. (Color online) Third simulation. Evolution of energy spectrum $E(k)$ vs wave number k. The setup is as in the first simulation (vortex rings of random radius and traveling in the x direction are injected), but the LIA replaces the Biot-Savart law. In this way vortex lines interact only when they reconnect. Note again the transfer of energy from large k to small k.

$E(k)$ during the initial evolution and the overall buildup of $K(t)$ [the area under $E(k)$]. The dashed line is the spectrum of the forcing term $\mathbf{v}_{\rm ext}$. The transfer of energy from large k near the forcing k_f to small k is apparent: At small k, $E(k)$ grows by a factor of 500.

In the third numerical simulation [35] we examine the role of reconnections. We proceed as in the first simulation, injecting rings of random radius aligned in the yz plane and traveling in the x direction; we retain the reconnection algorithm, but replace the Biot-Savart law (1b) with its local induction approximation (LIA) [36,37]

$$\mathbf{v}(\mathbf{s},t) \approx \frac{\kappa}{4\pi} \ln (R/a_0) \mathbf{s}' \times \mathbf{s}'', \tag{3}$$

where a prime denotes a derivative with respect to arc length and $R = 1/|\mathbf{s}''|$ is the local radius of curvature. Under the LIA, vortex lines move along the binormal direction with speed inversely proportional to R, ignoring each other; in other words, vortices interact only when they collide. Figure 4 shows that, in the absence of forcing, $K(t)$ decreases, but energy is shifted from large k to small k, as in the previous simulations. This result means that vortex-vortex interaction (represented by the Biot-Savart law) is not necessary to produce a reverse energy transfer: Vortex reconnections are enough to drive the process.

A simple geometrical interpretation of this result is the following. The energy and speed of a vortex loop of size R are roughly proportional to R and $1/R$, respectively. Vortex loops traveling parallel or antiparallel to a given direction undergo two kinds of collisions: head-on and from behind. Head-on collisions leave the size of loops approximately unchanged after the reconnection, as in Fig. 5; collisions from behind create a larger loop and a smaller loop, as in Fig. 6. The large loop, which contains most of the energy, is more likely to become entangled with other vortices, while the small loop, which quickly moves away, is more likely to be absorbed by walls (in the presence of periodic boundary conditions, the small loops that collide with larger loops can only become smaller, without significantly increasing the size of the larger loops). In an isotropic tangle, collisions of either kind are equally likely. In an anisotropic system (a jet of rings, or a system in which loops are injected along a preferred direction), we expect more collisions from behind, particularly in the early stage, hence a shift of energy to larger length scales induced by reconnections alone.

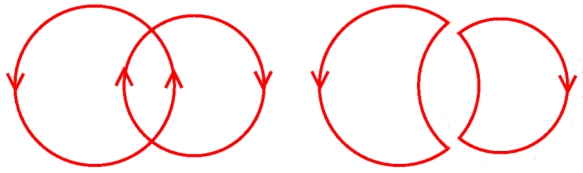

FIG. 5. (Color online) Schematic head-on collision of vortex loops traveling in opposite directions. After reconnection, the loops have essentially the same size.

In the fourth simulation [38] we proceed as in the first: We inject rings moving in the x direction continually (drawing their radius from a normal distribution and computing the evolution using the Biot-Savart law and the reconnection algorithm); the difference is that now the forcing is larger than in the first simulation [39]. When the vortex line density saturates, the tangle settles down to a steady state (a snapshot of the saturated vortex tangle is shown in Fig. 7). We notice (see Fig. 8) that so much energy has been shifted to wave numbers smaller than the injection's inverse length scale $k_f \approx 1/\bar{R}$ that the spectrum has acquired a form that is consistent with the classical Kolmogorov scaling $E(k) \sim k^{-5/3}$ typical of ordinary turbulence, a result that is in agreement with existing numerical simulations of superfluid turbulence [40–44].

Now we put these numerical results in the context of experiments. Walmsley and Golov [32] created turbulence in ^{4}He at very low temperatures (so the normal fluid can be neglected) by injecting vortex rings with a high-voltage tip. After the injection stage, they monitored the decay of the vortex line density L and observed two regimes, $L \sim t^{-1}$ (called ultraquantum) and $L \sim t^{-3/2}$ (called quasiclassical), associated with short and long initial injection times, respectively. Both regimes were also observed in ^{3}He-B [45]. In our previous paper [46] we modeled the experiment of Walmsley and Golov as realistically as possible, numerically injecting vortex rings in the form of a narrow beam originating from a point source. First, we reproduced ultraquantum and quasiclassical regimes

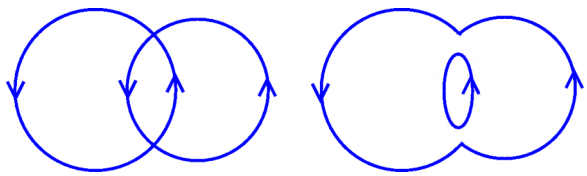

FIG. 6. (Color online) Schematic collision of loops traveling in the same direction. After the reconnection, the loops have very different sizes.

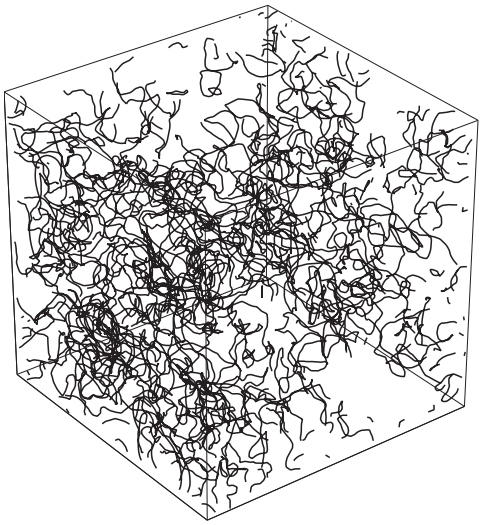

FIG. 7. Fourth numerical simulation. Snapshots of the vortex tangle in the steady-state regime at $t = 15$ s ($L \approx 160$ cm^{-2}).

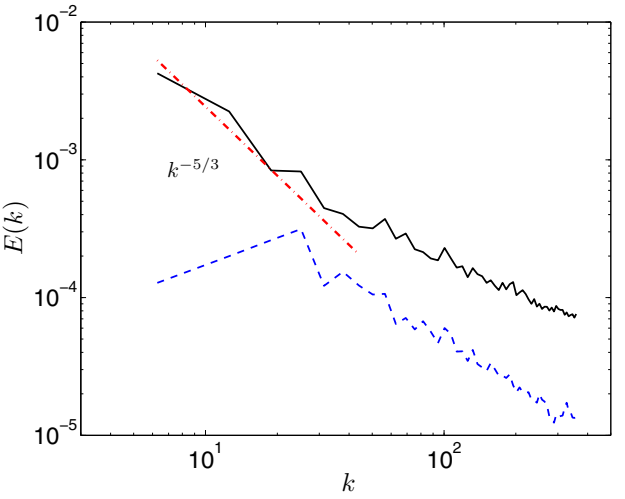

FIG. 8. (Color online) Fourth simulation. Energy spectrum $E(k)$ (arbitrary units) vs wave number k (cm^{-1}) at $t = 0.75$ s and $L = 43.9$ cm^{-2} (dashed blue line) and $t = 15$ s and $L = 159.6$ cm^{-2} (solid black line). The dot-dashed line shows the $k^{-5/3}$ Kolmogorov scaling.

at short and long injection times (in a related calculation [47], vortex injection was not strong enough to generate large length scales; this is consistent with the facts that turbulence decayed as $L \sim t^{-1}$ and the relative forcing [39] was one-tenth that in our first simulation). Second, by computing the spectrum, we discovered [46] that the quasiclassical regime is the decay of a Kolmogorov spectrum, which forms as energy is transferred from the small injection length scale to larger length scales. However, the nonuniformity of the beam was (at least in principle) a possible origin of the observed inverse energy transfer.

In summary, the simulations that we present here, together with our previous result [46], show clearly the phenomenon of energy transfer from small to large scales and its relation with vortex reconnections. The negative energy flux is observed not only in transients but also in statistically-steady-state regimes and occurs over a wide range of wave numbers. The effect that we describe has implications for other superfluid turbulence experiments, in particular for the formation of developed turbulence past a grid, as in the towed-grid experiments by Smith *et al*. [48], which have been much discussed in the literature, the oscillating grid experiments performed by Bradley *et al*. [45,49], and the most recent experiments of Walmsley *et al*. [50], which seem to confirm the inverse transfer of energy that we have identified.

The analogies with related processes in classical fluid dynamics are also intriguing, but need further detailed investigation. It is interesting to recall recent work by Biferale *et al*. [51], who numerically induced the classical three-dimensional inverse energy cascade by artificially restricting the nonlinearity of the governing Navier-Stokes equation to the interaction of Fourier modes of the same helical sign. Their result shows that, in principle, all three-dimensional turbulent flows contain nonlinearities that may lead to an inverse cascade: To make the effect apparent one has to break the mirror symmetry of the interactions. Our findings are apparently consistent with those of Biferale *et al*. It must be stressed that it is not the anisotropy of the configuration that matters, but rather the anisotropy of the interaction. In the problem of Biferale *et al*., the anisotropy is enforced at every time step by the numerical algorithm; in our problem, the anisotropy is introduced by the initial condition that favors one kind of vortex reconnections over the other, as we have described. In more isotropic conditions, the direct cascade generally may hide this effect (for example, a small inverse energy transfer is apparent in the energy spectrum of a decaying Taylor-Green flow [52], although the authors do not comment on it).

In conclusion, the natural question is whether the inverse energy transfer that we have described amounts to a cascade or creates an equilibrium distribution at large scales as described, for example, in the simpler case of wave turbulence [53]. In a nonlinear system we expect that excitation in a spectral interval means transfer of energy to both larger and smaller scales. In our case, the interaction between vortex loops is not symmetric and far from trivial. Numerical simulations over a much wider range of wave numbers and temporal scales than we can perform now will help answer this question.

We acknowledge fruitful discussions with W. F. Vinen, L. Skrbek, A. Golov, J. Laurie, P. Clark, and S. Nazarenko and the financial support of the Leverhulme Trust, the EPSRC, and the Carnegie Trust.

[1] L. F. Richardson, *Weather Prediction by Numerical Process* (Cambridge University Press, Cambridge, 1922).
[2] R. H. Kraichnan and D. Montgomery, Rep. Prog. Phys. **43**, 547 (1980).
[3] P. Tabeling, Phys. Rep. **362**, 1 (2002).
[4] B. Galanti and P.-L. Sulem, Phys. Fluids A **3**, 1778 (1991).
[5] D. Hefer and V. Yakhot, Phys. Fluids A **1**, 1383 (1989).

[6] V. Yakhot and R. Pelz, Phys. Fluids **30**, 1272 (1987).
[7] V. Yakhot and G. Sivashinsky, Phys. Rev. A **35**, 815 (1987).
[8] P. D. Mininni and A. Pouquet, Phys. Fluids **22**, 035105 (2010).
[9] A. Pouquet, A. Sen, D. Rosenberg, P. D. Mininni, and J. Baerenzung, Phys. Scr. **2013**, 014032 (2013).
[10] L. M. Smith and F. Waleffe, Phys. Fluids **11**, 1608 (1999).
[11] H. Xia, H. Punzmann, G. Falkovich, and M. G. Shats, Phys. Rev. Lett. **101**, 194504 (2008).
[12] P. S. Marcus, Nature (London) **331**, 693 (1988).
[13] J. Sommeria, S. D. Meyers, and H. L. Swinney, Nature (London) **331**, 689 (1988).
[14] L. Skrbek and K. R. Sreenivasan, Phys. Fluids **24**, 011301 (2012).
[15] J. Koplik and H. Levine, Phys. Rev. Lett. **71**, 1375 (1993).
[16] M. Kursa, K. Bajer, and T. Lipniacki, Phys. Rev. B **83**, 014515 (2011).
[17] S. Zuccher, M. Caliari, and C. F. Barenghi, Phys. Fluids **24**, 125108 (2012).
[18] M. S. Paoletti, M. E. Fisher, and D. P. Lathrop, Physica D **239**, 1367 (2010).
[19] R. M. Kerr, Procedia IUTAM **9**, 57 (2013).
[20] K. W. Schwarz, Phys. Rev. B **38**, 2398 (1988).
[21] P. G. Saffman, *Vortex Dynamics* (Cambridge University Press, Cambridge, 1992).
[22] The opening angle of the tree algorithm is 0.3.
[23] A. W. Baggaley and C. F. Barenghi, Phys. Rev. B **84**, 020504 (2011).
[24] A. W. Baggaley and C. F. Barenghi, J. Low Temp. Phys. **166**, 3 (2012).
[25] A. W. Baggaley, J. Low Temp. Phys. **168**, 18 (2012).
[26] W. F. Vinen, Phys. Rev. B **64**, 134520 (2001).
[27] A. W. Baggaley and C. F. Barenghi, Phys. Rev. B **83**, 134509 (2011).
[28] G. Krstulovic, Phys. Rev. E **86**, 055301(R) (2012).
[29] S. Nazarenko, *Wave Turbulence*, Springer Lecture Notes in Physics Vol. 825 (Springer, Berlin, 2011).
[30] W. F. Vinen, M. Tsubota, and A. Mitani, Phys. Rev. Lett. **91**, 135301 (2003).
[31] The parameters are $D = 0.1$ cm, $\delta = 10^{-3}$ cm, rings injected with frequency $f = 10^3$ Hz, mean radius $\bar{R} = 0.0024$ cm, and standard deviation $\sigma = 5 \times 10^{-4}$ cm.
[32] P. M. Walmsley and A. I. Golov, Phys. Rev. Lett. **100**, 245301 (2008).
[33] Spectra are computed from a 512^2 Cartesian mesh in the xz plane.
[34] The parameters are $D = 1$ cm and $\delta = 0.01$ cm.
[35] The parameters are as in [34].
[36] L. Da Rios, Rend. Circ. Mat. Palermo **22**, 117 (1906).
[37] R. L. Ricca, Fluid Dyn. Res. **18**, 245 (1996).
[38] The parameters are $D = 1$ cm, $\delta = 0.01$ cm, rings injected with frequency $f = 125$ Hz, mean radius $\bar{R} = 0.021$ cm, and standard deviation $\sigma = 0.017$ cm.
[39] Let D be the unit of length and κ/ℓ the unit of speed. The unit of time is then $\tau = D\ell/\kappa$. In a characteristic time scale τ, the injected vortex length relative to the total vortex length (using length as a proxy for energy for simplicity) $\delta\Lambda/\Lambda = 2\pi\bar{R}f\tau/\Lambda$ is almost three times larger in the fourth simulation than in the first.
[40] C. Nore, M. Abid, and M. E. Brachet, Phys. Rev. Lett. **78**, 3896 (1997).
[41] T. Araki, M. Tsubota, and S. K. Nemirovskii, Phys. Rev. Lett. **89**, 145301 (2002).
[42] M. Kobayashi and M. Tsubota, Phys. Rev. Lett. **94**, 065302 (2005).
[43] N. Sasa, T. Kano, M. Machida, V. S. L'vov, O. Rudenko, and M. Tsubota, Phys. Rev. B **84**, 054525 (2011).
[44] A. W. Baggaley, C. F. Barenghi, A. Shukurov, and Y. A. Sergeev, Europhys. Lett. **98**, 26002 (2012).
[45] D. I. Bradley, D. O. Clubb, S. N. Fisher, A. M. Guénault, R. P. Haley, C. J. Matthews, G. R. Pickett, V. Tsepelin, and K. Zaki, Phys. Rev. Lett. **96**, 035301 (2006).
[46] A. W. Baggaley, C. F. Barenghi, and Y. A. Sergeev, Phys. Rev. B **85**, 060501 (2012).
[47] S. Yamamoto. M. Tsubota, and W. F. Vinen, J. Phys. C: Conf. Ser. **400**, 012075 (2012).
[48] M. R. Smith, R. J. Donnelly, N. Goldenfeld, and W. F. Vinen, Phys. Rev. Lett. **71**, 2583 (1993).
[49] D. I. Bradley, D. O. Clubb, S. N. Fisher, A. M. Guénault, R. P. Haley, C. J. Matthews, G. R. Pickett, V. Tsepelin, and K. Zaki, Phys. Rev. Lett. **95**, 035302 (2005).
[50] P. M. Walmsely, P. A. Tomsett, D. E. Zmeev, and A. I. Golov, arXiv:1308.6171.
[51] L. Biferale, S. Musacchio, and F. Toschi, Phys. Rev. Lett. **108**, 164501 (2012).
[52] T. Araki, M. Tsubota, and S. Nemirovskii, J. Low Temp. Phys. **126**, 303 (2002).
[53] E. Balkovsky, G. Falkovich, V. Lebedev, and I. Ya. Shapiro, Phys. Rev. E **52**, 4537 (1995).